Control of organic–inorganic halide perovskites in solid-state solar cells: a perspective

ARTICLE · FEBRUARY 2015

DOI: 10.1007/s11434-015-0734-y

4 AUTHORS:

Qiong Wang
University of Queensland
10 PUBLICATIONS **50** CITATIONS
SEE PROFILE

Hongjun Chen
University of Queensland
54 PUBLICATIONS **1,570** CITATIONS
SEE PROFILE

Gang Liu
Chinese Academy of Sciences
98 PUBLICATIONS **7,859** CITATIONS
SEE PROFILE

Lianzhou Wang
University of Queensland
217 PUBLICATIONS **5,311** CITATIONS
SEE PROFILE

Sci. Bull. (2015) 60(4):405–418
DOI 10.1007/s11434-015-0734-y

www.scibull.com
www.springer.com/scp

Review

Materials Science

Control of organic–inorganic halide perovskites in solid-state solar cells: a perspective

Qiong Wang · Hongjun Chen · Gang Liu · Lianzhou Wang

Received: 9 December 2014 / Accepted: 24 December 2014 / Published online: 4 February 2015

Abstract Since the year of 2009 when the first application of organohalide lead perovskite as the light harvester in solar cells was reported, tremendous attention has been devoted to these new types of perovskite-based solid-state solar cells and remarkable power conversion efficiency of over 20 % has been achieved to date. In this review, we first introduce the properties of organic–inorganic halide perovskites and then focus on the notable achievements made on the perovskite layer to improve the power conversion efficiency of solid-state perovskite solar cells, which is featured by process engineering of the state-of-the-art lead methylammonium triiodide perovskite and material control of lead triiodide perovskites and other newly emerged perovskites. In the end, we wish to provide an outlook of the future development in solid-state perovskite solar cells. Provided that the instability and toxicity of solid-state perovskite solar cells can be solved, we will witness a new era for cost-effective and efficient solar cells.

Keywords Perovskite solar cells · Fabrication procedures · High performance

Q. Wang · H. Chen · L. Wang (✉)
Nanomaterials Centre, School of Chemical Engineering and Australian Institute for Bioengineering and Nanotechnology, The University of Queensland, Brisbane QLD 4072, Australia
e-mail: l.wang@uq.edu.au

G. Liu (✉)
Shenyang National Laboratory for Materials Science, Institute of Metal Research, Chinese Academy of Sciences, Shenyang 110016, China
e-mail: gangliu@imr.ac.cn

1 Introduction

Perovskites can generally be expressed as AMX_3, where A stands for an organic or inorganic cation, M is a metal ion and X is an anion [1]. The crystallographic stability is influenced by a tolerance factor t and an octahedral factor u [2]. For the organohalide metal perovskite of present interest, A is an organic cation, and X is halide anion. The most commonly used perovskite in the state-of-art solid-state solar cells is $CH_3NH_3PbI_3$ ($MAPbI_3$), where A is $CH_3NH_3^+$, M is Pb^{2+} and X is I^- (Fig. 1). The crystal structures of perovskites can be transited between cubic, tetragonal and orthorhombic depending on the temperature [3, 4]. Many well-known perovskites are fully inorganic, e.g., $BaTiO_3$ [5], $BiFeO_3$ [6] or $SrTiO_3$ [7], and they are featured by piezoelectric or ferroelectric properties and abnormal photovoltaic effect [8–10]. At present, the ferroelectric property of organohalide lead perovskites and observed hysteresis in photovoltaic performance in perovskite solar cells are still under debate [11–16].

Organic–inorganic lead perovskites recalled attentions from photovoltaic area began with the application of them as light absorbers in dye-sensitized solar cells (DSCs) in 2009. Miyasaka's group [17] pioneered the first perovskite solar cells where $MAPbX_3$ (X = I, Br) were loaded on top mesoporous TiO_2 photoanodes by dropping $MAPbX_3$ (X = I, Br) solutions on TiO_2 photoanodes and spin cast. However, compared with DSCs based on ruthenium sensitizer [18–21] or porphyrin sensitizer [22–24], the resulting power conversion efficiencies (PCEs) were quite poor (3.81 % for $MAPbI_3$ and 3.13 % for $MAPbBr_3$). One of the reasons for its poor performance may be determined by its configuration. In a sandwich-type open cell, liquid electrolyte was dropped between two electrodes, and the contact

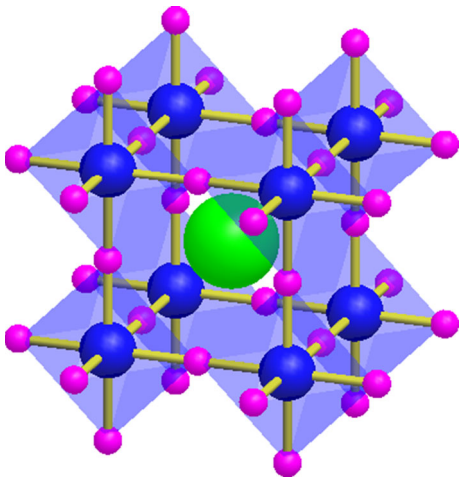

Fig. 1 Cubic crystal structures of $MAPbI_3$ perovskite where the organic group MA^+, inorganic metal Pb^{2+} and halide I^- occupy positions A (green), B (blue) and X (pink), respectively

between electrons and liquid electrolyte is not as good as that in a sealed solar cells. Later, Park's group [25] chose $MAPbI_3$ as light absorber in sealed DSCs with thinner TiO_2 photoanodes and investigated the performance of DSCs with different concentrations of $MAPbI_3$ in solutions. In their case, self-made liquid electrolyte was introduced into the system via vacuum back-filling method, following the procedures used for the assembly of conventional DSCs [26]. Although their work boosted the performance of $MAPbI_3$-based DSCs, the liquid electrolyte was demonstrated to be corrosive for $MAPbX_3$ (X = I, Br).

The real breakthrough came when Kim et al. [27] used $MAPbI_3$ as a light absorber in combination with the solid-state hole conductor, 2,2′,7,7′-tetrakis-(*N*,*N*-dimethoxyphenylamine)-9,9′-spirobifluorene (spiro-OMeTAD). A PCE of 9.7 % was achieved with much better stability compared with its liquid counterparts. Soon after that, Lee et al. [28] introduced meso-superstructure solar cells where mesoporous layer was composed of insulator Al_2O_3, instead of TiO_2. It was studied that Al_2O_3 mesoporous layer worked as a scaffold for more loading of $MAPbI_3$ perovskite. Since then, there have been exponentially increased research effort devoted to this field, and there were also a number of excellent review articles published in the relevant fields [29–32]. However, to date no review article has put particularly focus on control of the perovskite layer in terms of morphology and materials engineering. In this review, we firstly introduced the general properties of $MAPbX_3$ (X = Cl, Br, I) perovskites, the structure and components of perovskite solid-state solar cells, and then elaborated various fabrication procedures for the preparation of perovskite films and their influences on the morphology of perovskite film and performance of solar cells. Recent works on lead-free perovskites were also discussed. In the end, we summarized some most useful and facile methods for deposition of organic–inorganic halide perovskites based on our experiment and experience, and we prospected that development of lead-free perovskites with high stability would be the next breakthrough in this area.

1.1 Optical properties of $MAPbX_3$ (X = Cl, Br, I) perovskites

Different from all inorganic perovskites that generally have a large indirect energy band gap of around 3 eV [33, 34], three-dimensional (3D) organic–inorganic halide perovskites exhibit strong absorbance in the visible wavelength range with a direct energy band gap of around ~1.5 eV for $MAPbI_3$ and huge absorbance coefficient of one order of magnitude higher than that of traditional dye sensitizers [27]. By adjusting the ratio of halide in a hybrid perovskite ($MAPbX_3$, X = Br or I), the energy band gap and absorbance spectra of perovskites can be easily tuned [35]. Initially, researchers have investigated the luminescent properties of two-dimensional (2D) layer structures [36–38]. It was soon discovered that the 3D perovskites can also exhibit broad and strong photoluminescence (PL) [39]. PL quantum efficiencies of up to 70 % have been observed for solution-processed $MAPbI_{3-x}Cl_x$ perovskite films [40]. It was also reported that the PL emission wavelengths and electron lifetimes can be affected by the halide in $MAPbX_3$ perovskites [41–44].

1.2 Electronic properties of $MAPbX_3$ (X = Cl, Br, I) perovskites

In addition to special optical properties, their unique electronic properties also contribute to their success in perovskite solar cells. It was reported that the electron-hole diffusion length of mixed halide ($MAPbI_{3-x}Cl_x$) and triiodide ($MAPbI_3$) perovskite absorbers was in orders of micrometer and few hundred nanometers [43, 44]. Moreover, by reducing non-radiative electron-hole recombination within $MAPbI_{3-x}Cl_x$ perovskite using Lewis bases thiophene and pyridine, Noel et al. [45] can improve its PL lifetimes by nearly an order of magnitude. Besides, these 3D organohalide lead perovskites exhibit high hole mobility of around 60 $cm^2/(V\ s)$ [46]. Thus, efficient perovskite solar cells can be made without any hole transporter materials due to the ambipolar semiconducting nature of perovskite [47, 48]. By mapping the variation in efficiency of charge separation and collection across the perovskite solar cells, Edri et al. [49] revealed two important interfaces, one at/near the absorber/hole transport material (HTM) and the other at/near the absorber/electron transport material (ETM). Their work implies that the perovskite solid-state solar cells operate as a p-i-n device similar to amorphous silicon-based solar cells. In

our reported work [50], we also demonstrated that by dissolving MAI and $PbCl_2$ in DMF solvent, a functional electrolyte for DSCs can be prepared.

1.3 Structure of perovskite solid-state solar cells

The structure of perovskite solar cells can be illustrated in Fig. 2. For a planar-structured solar cell, there is only one compact layer that is generally composed of TiO_2, and no mesoporous layer is involved [51]. For a mesoporous-structured solar cell, on top of the compact layer, there is always a mesoporous layer that is generally composed of TiO_2 or ZnO [27, 52–57]. For the mesoporous layer composed of an insulator, such as Al_2O_3 or SiO_2, it is called "meso-superstructured" solar cells [28]. It has been investigated that electron diffusion length in $MAPbI_3$ is shorter than hole diffusion length; therefore, a mesoporous layer of electron selective layer is generally needed for $MAPbI_3$ mesoporous solar cells [58]. However, a planar structure is preferred for $MAPbI_{3-x}Cl_x$ solar cells because the electron and hole diffusion length are competitive with each other in $MAPbI_{3-x}Cl_x$ perovskite [31].

1.4 Components of perovskite solid-state solar cells

In general, perovskite solar cells have three key components, i.e., photoanode, perovskite layer and hole transporter. However, different from DSCs [59–64], the nanostructure of the photoanode material is not that important, because the organohalide lead perovskite itself has a much higher absorbance coefficient [65] and thus even a thin layer of around 100 nm is enough to obtain a considerable high performance [66]. On the other hand, the barrier layer or the underlayer of TiO_2 plays a more crucial role in the performance of solid-state solar cells [67–69]. Different methods or techniques applied to make a pin-hole free compact layer have been thoroughly studied previously for dye-sensitized solid-state solar cells [70]. Also, organic [71–74] or inorganic hole transporters [75, 76] have been widely studied in organic solar cells [77–79], solid-state DSCs [80–83] and extremely thin absorber solar cells [84–87]. Interestingly, it has been recently reported that the ambipolar semiconducting nature of perovskite enabled the configuration of comparative solid-stated solar cells without any electron transport layer [88] or hole transport layer [48, 89–92]. Therefore, here we will mainly discuss progresses made to the perovskite layer in terms of the newly emerged perovskite solid-state solar cells.

2 Morphology control of perovskite film

Although the perovskite layer can be easily prepared by solution-processed method, it has been widely reported that one-step spin-coating method generally results in a non-uniform and nonconstant film, leaving the direct contact between the electron transporting layer and the hole transporting layer [93, 94].

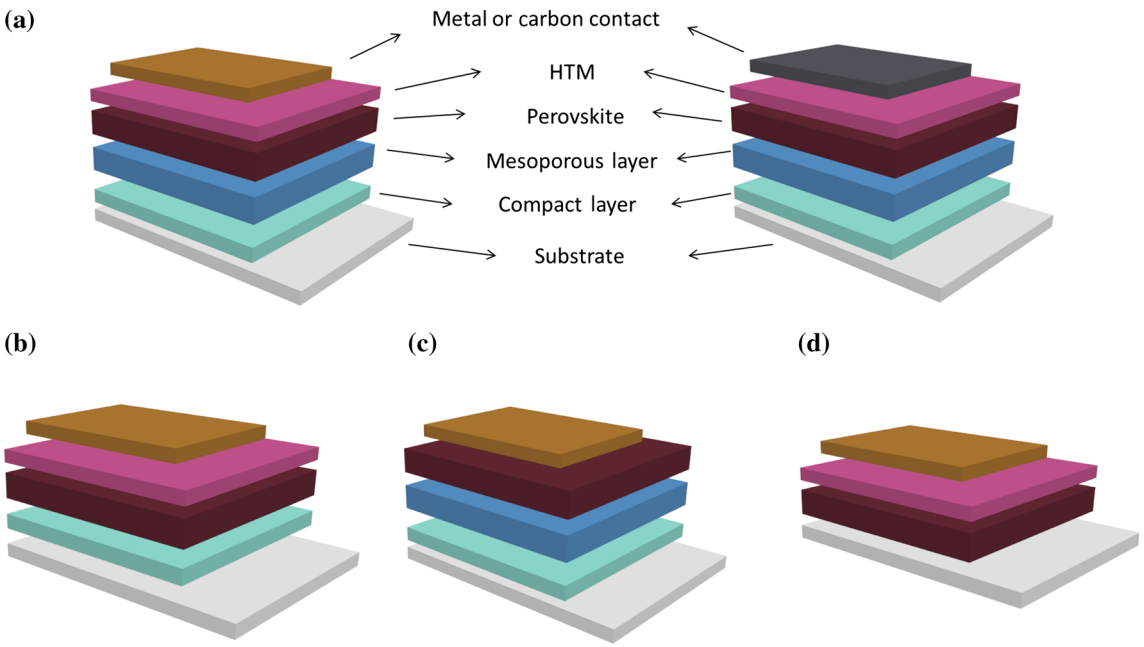

Fig. 2 Configuration of perovskite solid-state solar cells. **a** Mesoporous-structured solar cells when mesoporous layer is composed of semiconductors, such as TiO_2 and ZnO, or meso-superstructured solar cells when mesoporous layer is composed of insulators, such as Al_2O_3; **b** planar-structured solar cells that do not contain mesoporous layer; **c** hole conductor free solar cells; **d** electron transport layer free solar cells

2.1 Sequential deposition method

To create a uniform and flat perovskite film, many methods have been developed. Burschka et al. [95] proposed a two-step method that involves spin-coating the hot inorganic crystal (PbI_2) in *N*,*N*-dimethylformamide (DMF) on the photoanode first and then immersing the photoanode into CH_3NH_3I (MAI)-isopropanol (IPA) solution, which generates a uniform and fully covered $MAPbI_3$ film. The first perovskite solar cells with a PCE of 15 % [95] was achieved using this method compared with 9 % [27] that was reported using one-step spin-coating method. PCE of over 10 % [89, 91] in hole conductor free perovskite solar cells has been achieved using this method compared with an initial value of 7.3 % [47]. It has been demonstrated that this method is more suitable for mesoporous-structured solar cells where the mesoporous layer formed by nanoporous network of TiO_2 can effectively confine PbI_2 nanocrystals to small sizes, where fully conversion of PbI_2 to $MAPbI_3$ perovskite only takes few minutes. However, when it is deposited on flat substrates, large PbI_2 crystals are formed and it makes it hard for organic ammonium to access and react with inner PbI_2, which results in that only the surface of the inorganic crystal layer is converted to the perovskite. Thus, full conversion of PbI_2 film to $MAPbI_3$ perovskite requires an extension of immersion time from several minutes to over 1 h, but it leads to the dissolution and/or pealing-off of the perovskite film into the solution [96]. Wu et al. [97] developed a modified sequential deposition method by using dimethylsulfoxide (DMSO) as the solvent to replace DMF. The strongly coordinative solvent of DMSO helps to retard the crystallization of PbI_2 film, and thus, in the sequential deposition process, such amorphous PbI_2 films can efficiently generate perovskite crystals with a full conversion within in 10 min. Moreover, in a planar-structured solar cell, the resultant perovskite showed a narrow distribution of perovskite particles sizes of around 200 nm and an average efficiency of 12.5 % was achieved. Bi et al. [98] modified the sequential deposition method by adding the treatment of dichloromethane directly after washing the perovskite film with IPA before the heat treatment. A smoother and more uniformly perovskite film was prepared in this method. A PCE of 13.5 % was obtained for mesoporous-structured solar cells.

2.2 Solvent engineering of one-step deposition

In addition to the efforts made on the control of the annealing temperature and annealing rate [94], many works have been done on the solvent engineering [99–101]. Jeon et al. [101] adopted a mixture of γ-butyrolactone (GBL) and DMSO to replace DMF as the solvent of hybrid perovskite, followed by a toluene drip while spinning. It was demonstrated that during the spin-coating process, GBL was evaporated first, and the toluene droplets facilitated the formation of a transitional phase, MAI-PbI_2-DMSO, that was discovered to play a crucial role in retarding the rapid reaction between PbI_2 and MAI. Then, the extremely homogeneous flat film was converted into a pure crystalline $MAPbI_3$ perovskite layer after annealing at 100 °C. Same method was applied to the preparation of $MAPb(I_{1-x}Br_x)_3$ perovskite, and a certified PCE of 16.2 % with no hysteresis was achieved using mesoporous-structured solar cells [101]. Xiao et al. [100] introduced the second solvent, chlorobenzene (CBZ), immediately after the spin-coating of $MAPbI_3$ from DMF solution before annealing at 100 °C for 10 min. It was found that this method could promote fast nucleation and growth of the perovskite crystals, which resulted in a uniform and closely packed $MAPbI_3$ perovskite films. Using this method, a PCE of 16.2 % under standard AM 1.5 sun was achieved in a planar-structured solar cells. However, it has been noted that the solvent engineering method is hard to repeat because the volume and timing of each drop of the solvent can have a significant influence on the product of the perovskite film.

2.3 Dual-source vapor deposition

Thin-film deposition of organic–inorganic hybrid perovskite had been reported early to be prepared by vapor deposition under vacuum via dual-source [102, 103] or single-source method [104]. Liu et al. [51] adopted this method to deposit a thin layer of $MAPbI_{3-x}Cl_x$ used in planar-structured solar cells, and a PCE of over 15 % was achieved. The advantage of this technique is that it has a better control of the film quality, thickness and morphology. However, it is often difficult to balance the organic and inorganic rates due to the significantly different vapor of $PbCl_2$ and MAI sources, which in turn determines the compositions of the resulting perovskite films. In addition, for each new organic–inorganic system, a reestablishment of the rates has to be carried out. It is even more problematic in some cases where some organic salts might not be thermally stable up to the temperatures required for evaporation [96]. Nevertheless, vapor deposition method exhibits a distinct advantage over solution processing method on the preparation of layered multi-stack thin films over large areas [51].

2.4 Other methods

Very recently, Chen et al. [105] developed a vapor-assisted solution process where PbI_2 framework film was formed by depositing precursor solution on the substrate and subsequently exposed it to MAI vapor (Fig. 3). This method

avoids the high reaction rate of perovskite during co-deposition of precursors and generates a uniform perovskite layer with large grains with reduced grain boundaries. Another quite interesting method is developed by Xiao et al. [106] who dissolved PbI_2 and MAI in separate solvents DMF and IPA, and then, different from sequential deposition method, each layer was deposited by spin-coating their precursor solution on the photoanodes with MAI layer on top of PbI_2 layer, and then, the perovskite layer was formed by interdiffusion of PbI_2/MAI films. Ono et al. [66] designed specially utilized equipment that could accurately control the flow and vapor pressure of MAI inside a vacuum chamber where the substrates deposited with PbI_2 were previously loaded. Although the improved two-step methods provided credits of generating the perovskite film of high quality and uniform, the general problem of this methodology is that the excess of either MAI or PbI_2 can form as an insulating layer that would largely increase the serial resistance of solar cells, which results in poor fill factor [106]. Another interesting and facile method was developed by Huang et al. [107] who introduced gas blowing after one-step spin-coating before heat treatment. Using this method, a uniform and densely packed perovskite films were formed and a PCE of 16.97 % was achieved in a planar structure solar cells.

3 Material engineering of organic–inorganic halide perovskites

As introduced in the beginning of this perspective, the absorbance properties and energy band gaps of perovskites can be significantly affected by the organic group, halide and inorganic metal. More than that, the morphology of perovskite films can also be influenced.

3.1 Incorporation of chlorine in triiodide perovskite films preparation

The incorporation of chlorine was firstly proposed by Lee et al. [28] who prepared the perovskite film spin casted from precursor solution that was composed of MAI:$PbCl_2$ = 3:1 in DMF solvent. By employing Al_2O_3 as the mesoporous "scaffold" in perovskite solar cells, a PCE of 10.9 % with a largely improved open-circuit photovoltage of over 1.1 V was achieved. It has been demonstrated that incorporation of chlorine inside $MAPbI_3$ perovskite improves the stability and changes the morphology of the resultant perovskite films [28, 45, 108–110]. More than that, $MAPbI_{3-x}Cl_x$ perovskite films prepared from $PbCl_2$-contained precursors require longer annealing time of around 45 min. In addition, the resultant X-ray diffraction (XRD) pattern of $MAPbI_{3-x}$

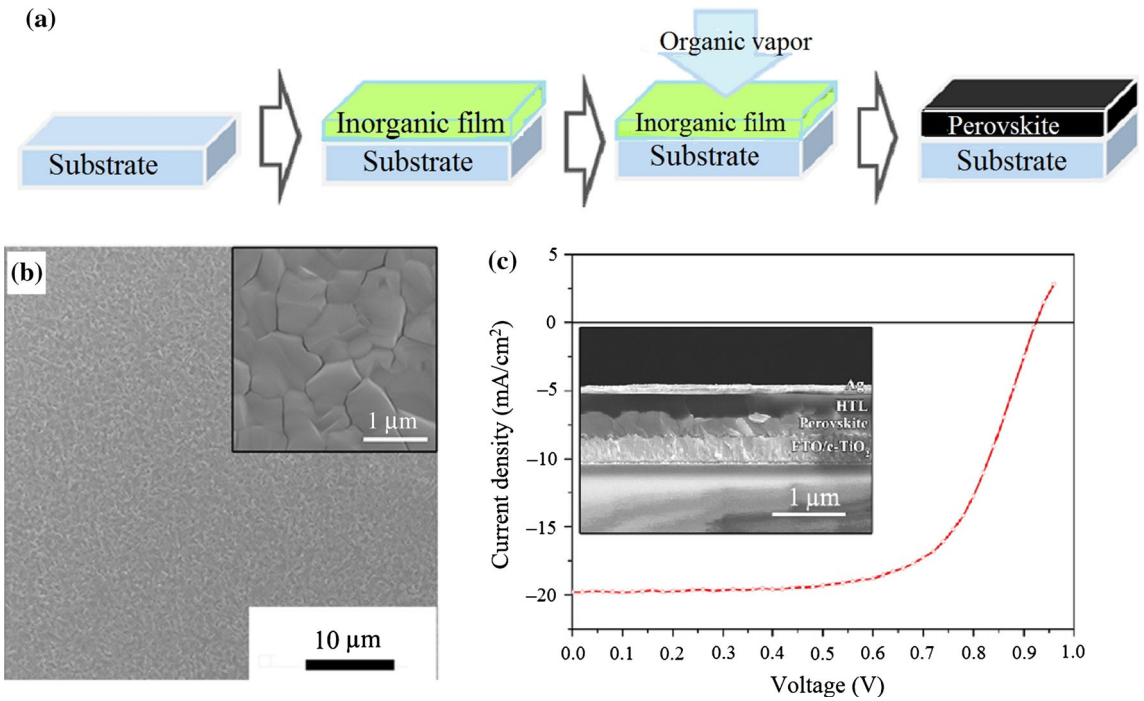

Fig. 3 (Color online) **a** Illustrations of perovskite films made through vapor-assisted solution process; **b** the resultant scanning electron microscope (SEM) image of perovskite films; **c** photovoltaic performance of solar cells. Reprinted with permission from Ref. [105]. Copyright 2013, American Chemical Society

Cl_x perovskite crystals is the same as that of $MAPbI_3$ [111], but exhibit much stronger peak intensity, which indicates enhanced crystallinity of the perovskites [112]. What's more, the diffusion length of charge carriers of $MAPbI_{3-x}Cl_x$ perovskite measured by transient absorption and photoluminescence-quenching techniques was greater than 1 μm, compared with that of around 100 nm for $MAPbI_3$ perovskite [43, 44]. Given the obvious differences on electronic properties, preparation procedures, crystallinity and morphology between $MAPbI_3$ and $MAPbI_{3-x}Cl_x$ perovskites, it has been measured by X-ray photoelectron spectroscopy (XPS) and energy dispersive spectroscopy (EDS) that there is barely no chlorine in the perovskite films deposited from chlorine-containing precursor solutions. Therefore, the formation process of perovskite films under the effect of chlorine is a topic worth of exploring (Fig. 4).

3.2 Bromine substitution of iodine in perovskite materials

Hybrid bromide and iodide lead perovskite were firstly studied by Noh et al. [35] who prepared $MAPb(I_{1-x}Br_x)_3$ perovskite films by one-step spin-coating from $MAPb(I_{1-x}Br_x)_3$ solutions that were made by mixing different ratios of $MAPbI_3$ and $MAPbBr_3$ solutions at 60 °C, followed by heated on a hot plate at 100 °C for 5 min. Besides changes in absorbance and energy band gaps of the resultant $MAPb(I_{1-x}Br_x)_3$ perovskite films, the XRD also revealed change in lattice parameters. It was later studied that different from chlorine atoms that preferentially occupy the apical positions in PbI_4X_2 octahedra, bromine atoms can occupy both apical and equatorial positions [114]. When $x = 0.2$ in $MAPb(I_{1-x}Br_x)_3$ perovskite as light absorber and polytriarylamine (PTAA) as hole transport material in mesoporous solar cells, a maximum PCE of 12.3 % was obtained (Fig. 5) [35]. Aharon et al. [115] prepared $MAPbI_xBr_{3-x}$ perovskite via sequential deposition methods where the dipping solution was composed of MAI and MABr under different molar ratios in IPA solvent. Changes in lattice parameters due to introducing of bromide ions were also observed in the XRD results. In hole conductor free solar cells (Fig. 6a), $MAPbI_xBr_{3-x}$ perovskite exhibited good hole conducting properties, where a PCE of 8.54 % and short-circuit current density (J_{sc}) of 16.2 mA/cm^2 was achieved. When iodine is completely substituted by bromine, tri-bromide perovskite $MAPbBr_3$ can be formed. The optical band gap is increased to 2.3 eV [116]. Chen et al. [117] assembled mesoporous solar cells using $MAPbBr_3$ perovskite that was deposited from $MAPbBr_3$ solution via one-step method as light absorber and *N*,*N*′-dialkyl perylenediimide (PDI) as hole conductor, achieving a high open-circuit voltage (V_{oc}) of around 1.3 V. Later, to further improve V_{oc}, Edri et al. [118] incorporated chloride

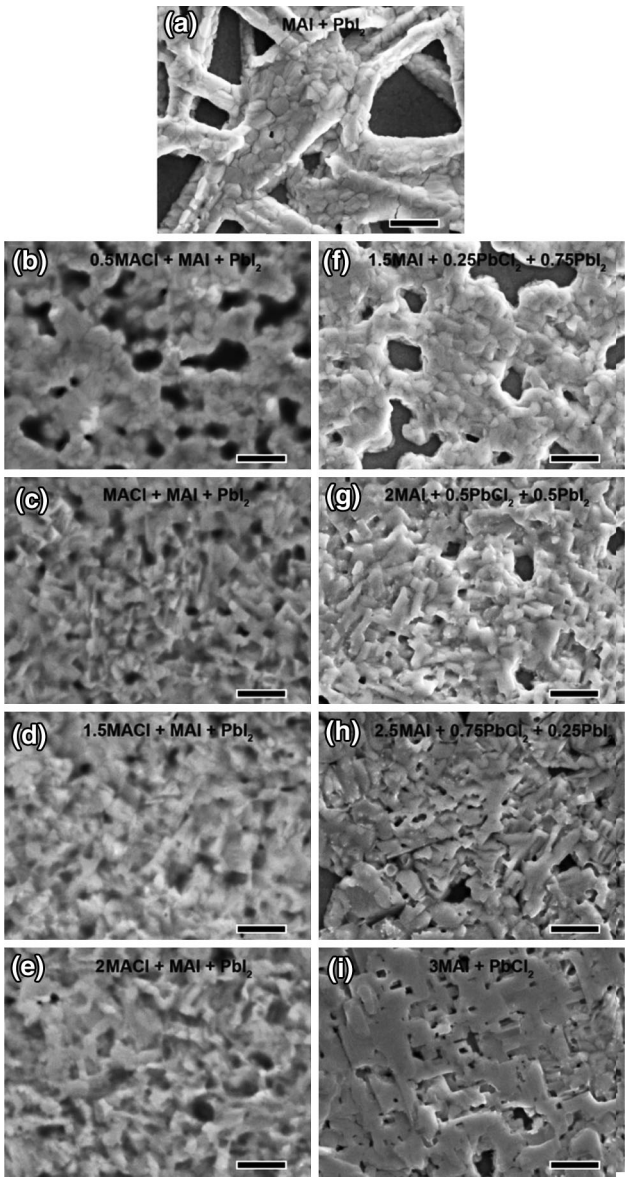

Fig. 4 Impact of solution chemistry on $MAPbI_{3-x}Cl_x$ film morphology. **a** Grown from a solution with equal molar ratio of MAI and PbI_2; **b–e** grown from solutions containing progressively increased MACl; **f–i** grown from solutions containing progressively increased quantities of $PbCl_2$. All scale bars are 1 μm. Reprinted with permission from Ref. [113]. Copyright 2014, American Chemical Society

into the lead bromide perovskite, an analog of $MAPbI_{3-x}Cl_x$, to possibly increase the diffusion lengths. However, the resultant XRD did not show any lattice parameter changes. Meanwhile, PDI was replaced by 4,4′-bis(*N*-carbazolyl)-1,1′-biphenyl (CBP) that was p-doped by bis(trifluoromethane)sulfonamide (LiTFSi) to adjust its highest occupied molecular orbital-lowest unoccupied molecular orbital (HOMO-LUMO) states to be better aligned with the valence and conduction band edges of $MAPbBr_{3-x}Cl_x$ perovskite. Finally, a V_{oc} of 1.5 eV was achieved, but the PCE was quite low of 2.7 % (Fig. 6b–d).

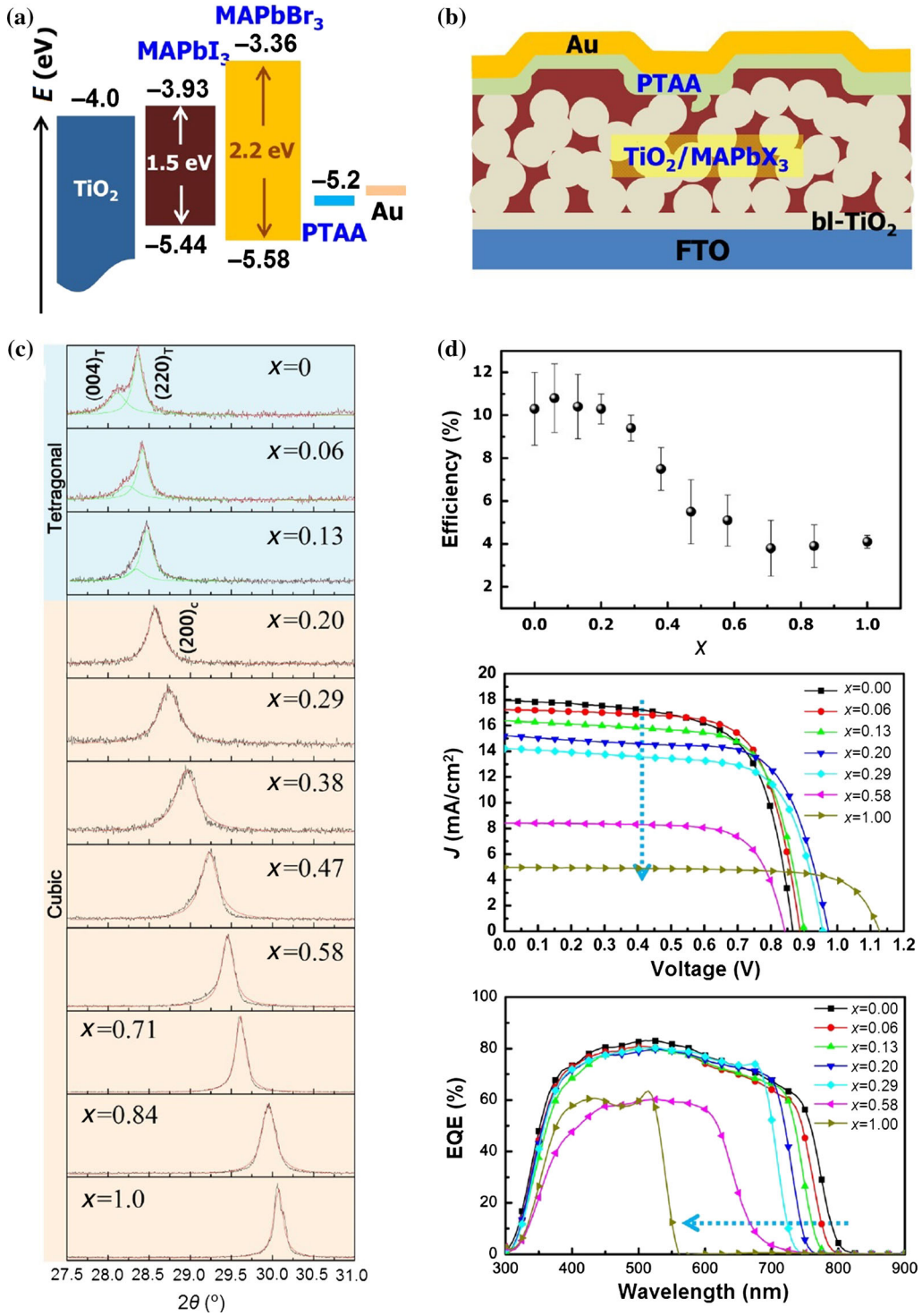

Fig. 5 TiO_2|$MAPb(I_{1-x}Br_x)_3$|PTAA|Au solar cells. **a** The energy alignment of components; **b** schematic structure; **c** changes in XRD patterns of $MAPb(I_{1-x}Br_x)_3$ perovskite due to incorporation of bromide; **d** influences of x in $MAPb(I_{1-x}Br_x)_3$ perovskite on PCE (top), photocurrent–voltage (J–V) curves (middle), and external quantum efficiency (EQE) (bottom). Reprinted with permission from Ref. [35]. Copyright 2013, American Chemical Society

3.3 Alternatives of organic groups in lead perovskites

As illustrated in the perovskite crystal structure in Fig. 1, the organic group in the ABX_3 structure also has influences in band gap of the perovskites. Particularly, the size of the organic group can cause the whole lattice to expand or contract, which in turn results in variation in band gap. However, if the organic group is too large, the 3D perovskite structure

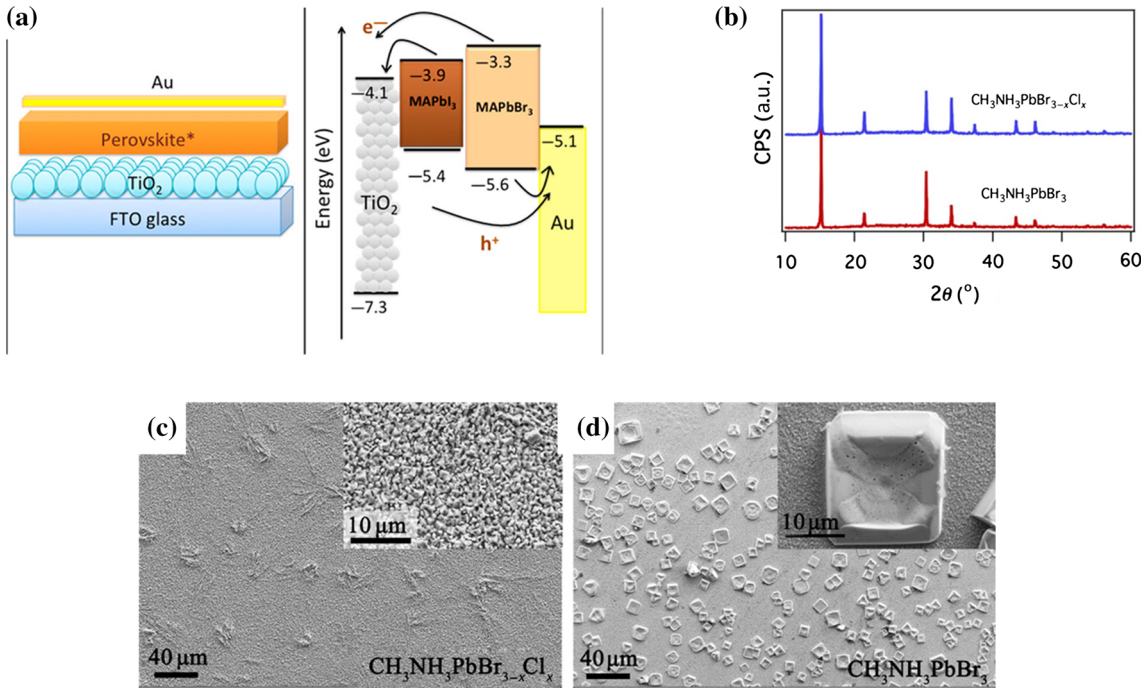

Fig. 6 (Color online) **a** Schematic structure of and energy alignment of components in TiO_2|$MAPbI_xBr_{3-x}$|Au solar cells. Reprinted with permission from Ref. [115]. Copyright 2014, American Chemical Society; **b** XRD patterns of $MAPbBr_3$ and $MAPbBr_{3-x}Cl_x$ perovskites. SEM images of $MAPbBr_{3-x}Cl_x$ (**c**) and $MAPbBr_3$ (**d**) perovskites in meso-superstructured solar cells. Reprinted with permission from Ref. [118]. Copyright 2014, American Chemical Society

would be unfavorable, which was constraint by the tolerance factor as we introduced previously. Layered perovskites will be formed when the organic group is big enough. Eperon et al. [119] synthesized ABX_3 perovskites of different A cations, methylammonium (MA^+, MA), cesium (Cs^+) and formamidinium ($HC(NH_2)_2^+$, FA). Compared to MA, Cs^+ has a smaller effective ionic radius, while FA has a slightly larger. Interestingly, it was observed that cesium lead triiodide ($CsPbI_3$) absorbs up to a shorter wavelength, whereas formamidinium lead triiodide ($FAPbI_3$) absorbs to a longer wavelength than methylammonium lead triiodide. As a result, $FAPbI_3$ is likely to be more competitive to be used as a light absorber in solar cells. However, perovskite films deposited directly from $FAPbI_3$ precursor solutions were discontinuous and coarse. A small amount of hydroiodic acid (HI) in its precursor solution helped to form extremely uniform and continuous films. $FAPbI_3$ perovskite films prepared by this method was used in thin-film planar-structured solar cells, and a high J_{sc} of over 23 mA/cm^2 and PCE of up to 14.2 % were achieved. Almost at the same time, Pang et al. [120] also reported this new perovskite. Differently, they prepared $FAPbI_3$ perovskite films via sequential deposition method where PbI_2 was spin casted from DMF solution on TiO_2 photoanodes, followed by dipping into FAI-contained IPA solution (Fig. 7a, b). In a mesoporous-structured solar cells using P3HT as the hole transport material, they achieved a PCE of 7.5 %. The low performance is possibly resulted from the fact that pristine P3HT is not an effective hole conductor.

Substitution of iodide with bromide was also investigated in formamidinium-based system. A broadly tunable light absorbance of $FAPbI_yBr_{3-y}$ perovskites was explored. XRD data of $FAPbI_yBr_{3-y}$ perovskites showed the shift of [100] (cubic) to the equivalent [110] (tetragonal) peak, which indicated the transition from a cubic (for $y < 0.5$, Br-rich) to a tetragonal ($y > 0.7$, I-rich) crystal structure [119]. Hanusch et al. [121] studied $FAPbBr_3$ perovskite prepared via sequential deposition method by immersing $PbBr_2$-coated TiO_2 photoanodes into FABr solution. The crystal structure and surface morphology of $FAPbBr_3$ were compared with $MAPbBr_3$ as shown in Fig. 8a. In planar heterojunction solar cells where $FAPbBr_3$ was used as light absorber and spiro-OMeTOD as hole conductor, a PCE of 6.5 % and J_{sc} of 6.6 mA/cm^2 were achieved (Fig. 8b). Hybrid lead perovskite, $FAPbI_{3-x}Cl_x$, was prepared by one-step spin-coating from DMF solution of FAI and $PbCl_2$ at a molar ratio of 3:1. Interestingly, a lower temperature was required for the annealing of $FAPbI_{3-x}Cl_x$ perovskite compared with $FAPbI_3$ perovskite films. In a mesoporous-structured solar cells with P3HT as hole conductor, a PCE of 7.5 % was measured for freshly made devices [122].

As we discussed previously, when the organic group, A cation, in ABX_3 structure is too large, layered perovskite

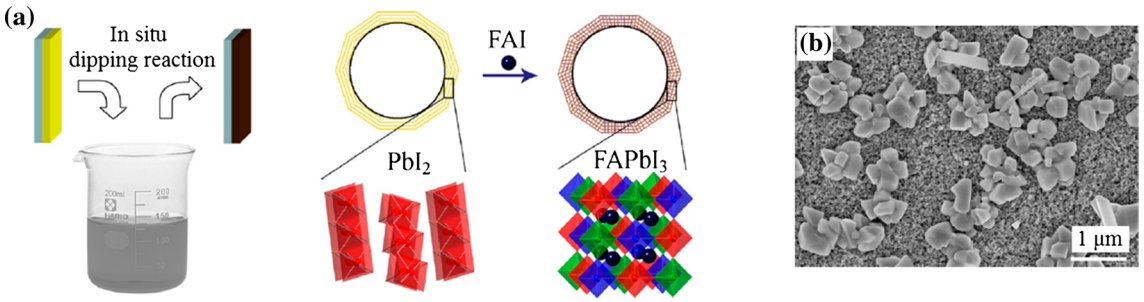

Fig. 7 **a** Illustration of in situ formation of $FAPbI_3$ via sequential deposition method; **b** the resultant surface morphology of perovskite film. Reprinted with permission from Ref. [120]. Copyright 2014, American Chemical Society

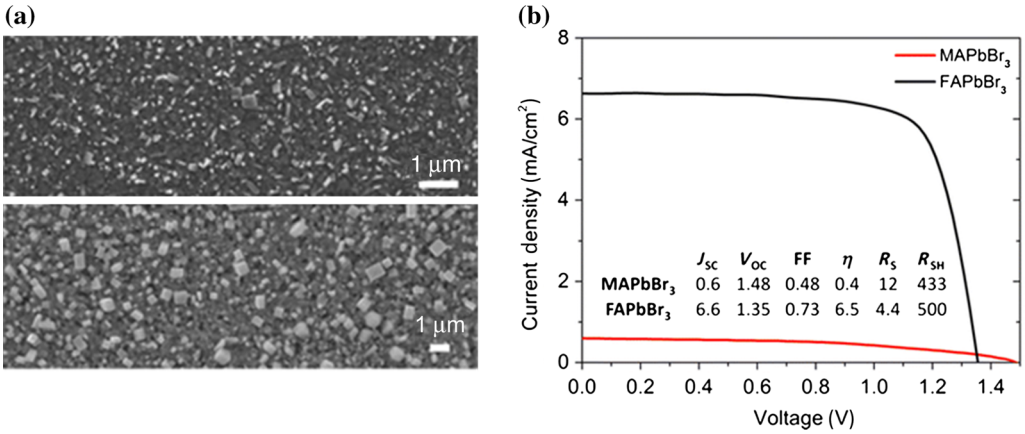

Fig. 8 **a** SEM surface images of $MAPbBr_3$ (top) and $FAPbBr_3$ (bottom) films; **b** *J–V* curves of $MAPbBr_3$ (red) and $FAPbBr_3$ (black) perovskites based solar cells. Inset table summarizes photovoltaic parameters (J_{sc}, V_{oc}, fill factor (FF), power conversion efficiency η, series resistance R_s (Ω cm^2) and shunt resistance R_{SH} (Ω cm^2)). Reprinted with permission from Ref. [121]. Copyright 2014, American Chemical Society

with 2D could be formed. Smith et al. [123] synthesized one 2D hybrid perovskite $(PEA)_2(MA)_2[Pb_3I_{10}]$ where PEA = $C_6H_5(CH_2)_2NH_3^+$. It was reported that $(PEA)_2(MA)_2[Pb_3I_{10}]$ films showed advantages in easier morphology as dense and fully covered films could be prepared via simply one-step spin-coating method. In planar heterojunction solar cells with spiro-OMeTAD as the hole transporter, a PCE of 4.73 % was achieved with a high V_{oc} of 1.18 V and a low J_{sc} of 6.73 mA/cm^2, which was determined by the slightly large band gap (~2.1 eV) of $(PEA)_2(MA)_2[Pb_3I_{10}]$ light absorber.

3.4 Lead-free perovskite and its photovoltaic applications

Although the performance of lead perovskites has been increased dramatically in recent 3 years, there is still a long way to go before the commercialization of perovskite solid-state solar cells. As addressed recently by Grätzel [124] in "The light and shade of perovskite solar cells", stability and toxicity are two big challenges. Identifying lead-free perovskites or other pigments that can replace $MAPbI_3$ is highly demanded for industrial applications. Motivated under this demand, lead-free perovskite, $MASnI_3$ was developed and applied in solar cells. Noel et al. [125] reported the first completely lead-free, $MASnI_3$ perovskite solar cells. Compared to lead perovskite, tin perovskite is highly instable in ambient atmosphere. Therefore, $MASnI_3$ perovskite solar cells were carried out all in a nitrogen-filled glovebox. Particularly, $MASnI_3$ perovskite was prepared by dissolving equimolar quantities of SnI_2 and MAI in degassed DMF and spin-coated onto desired substrates. Its absorbance spectra and PL were measured, and a sharp band edge at 1.23 eV was calculated. As a result, tin perovskite has a smaller band gap than lead perovskite, which indicates that the former has a broader spectrum response. Meanwhile, it was observed that at room temperature, tin perovskites formed crystals without any heat treatment. Tin perovskite-based solar cells were investigated using spiro-OMeTAD as hole conductor, a PCE of 6.4 % and J_{sc} of 16.8 mA/cm^2 were achieved. Compared with lead perovskite, the short-circuit current is comparatively low considering a smaller band gap of tin perovskite. The reason may be originated from

the short charge-diffusion length of around 30 nm of tin perovskite.

Optical absorbance and band gap of $MASnI_3$ perovskite were then engineered by inclusion of bromine. Hao et al. [126] prepared $MASnI_{3-x}Br_x$ compounds by mixing MAX and SnX_2 (X = Br, I) in a mortar and then sealed in silica ampules under vacuum, followed by heated at 200 °C. Interestingly, the series of compositions formed a continuous solid solution throughout its composition range, without presenting any structural transitions (at room temperature), thus retaining the crystal structure of both end materials. It was observed that the band gap of $MASnI_{3-x}Br_x$ perovskite was increased from 1.3 to 2.15 eV as more bromide was incorporated. Mesoporous-structured solar cells were prepared using $MASnI_{3-x}Br_x$ perovskite as absorbers and spiro-OMeTAD as hole. When $x = 2$, it achieved highest PCE of 5.73 % with the J_{sc} of 11.73 mA/cm^2, and V_{oc} as high as 0.82 V.

Another reported lead-free perovskite is $CsSnI_3$ [127]. Cs-based perovskite possesses a smaller band gap of 1.3 eV than $MAPbI_3$ (1.55 eV). The theoretical short-circuit photocurrent density of solar cells based on $CsSnI_3$ perovskite is 34.3 mA/cm^2 [128], compared to that of 25.9 mA/cm^2 of $MAPbI_3$ solar cells [32]. However, the prepared $CsSnI_3$ film is prone to contain intrinsic defects associated with Sn-cation vacancies that result in metallic conductivity [127]. Addition of SnF_2 was investigated to apply $CsSnI_3$ perovskite as a light absorber in solar cells by Kumar et al. [129]. SnF_2-$CsSnI_3$ samples were prepared by stoichiometric mixing of CsI, SnI_2 and SnF_2 in DMSO solvent and deposited by one-step spin-coating method, followed by 70 °C drying. The crystal structures of the serial compounds of SnF_2-$CsSnI_3$ exhibited similar XRD patterns, indicating no significant variation in lattice parameters. It was demonstrated that various solvents for SnF_2-$CsSnI_3$ compounds had crucial influences on the morphology of Cs-perovskite films. In the components of SnF_2-$CsSnI_3$ solar cells, 4,4′,4″-tris(*N*,*N*-phenyl-3-methylamino) triphenylamine (m-MEDATA) was used as HTM to match with the energy level of SnF_2-$CsSnI_3$ perovskite. Photovoltaic performance of devices fabricated with different SnF_2 concentrations and m-MTDATA as HTM was compared. It was demonstrated that the addition of SnF_2 into $CsSnI_3$ was critical in attaining decent photovoltaic performance through the reduction of Sn vacancies.

4 Summary and outlook

In summary, organic–inorganic hybrid perovskite materials combine the advantageous characteristics of crystalline inorganic solids and organic molecules within a molecular-scale composite, which endows the hybrid materials structural flexibility, magnetic, electronic and optical properties. Adjustments on the organic group, metal ions and halide can effectively affect the electronic property and optical property of the organic–inorganic hybrid perovskites; especially, larger size of organic cations can tune the crystal structure of hybrid perovskite from 3D to 2D. Generally, the direct band gap of organo-lead halide perovskite with large absorption coefficient makes it a promising candidate as a light absorber in solar cells. Depending on the configurations, perovskite solid-state solar cells can be divided into three types: planar-structured solar cells (planar heterojunction solar cells), mesoporous-structured solar cells and meso-superstructured solar cells. The development of solar cells with different configurations indicates improved understanding of the perovskite materials. The ambipolar semiconducting nature of lead perovskites extends its application from pristine light absorber to electron transporter and hole conductor.

Perovskite-based solid-state solar cells exhibit large V_{oc} when bromide ions are used to substitute iodide ions in perovskite structures. Large J_{sc} is expected for $MAPbI_3$ due to its low band gap of around 1.5 eV, but the perovskite film of high quality is normally required for devices of decent performance. Among all the methods developed for optimizing the morphology of $MAPbX_3$ (X = Cl, Br, I) perovskites, two-step sequential deposition method presents advantages in versatility and wide application for perovskites with different organic groups and halides. Dual-source vapor deposition has a sophisticated control of the crystallinity of $MAPbI_3$ perovskite, but it is not convenient to apply it to other perovskite materials. Solvent engineering of simple one-step deposition method and other methods apply facile ways to prepare perovskite of high quality, but they also limit themselves to certain perovskite materials. As a result, it is suggested that the reader should take advantages of each method and choose certain methods that are suitable and applicable to your unique cases.

To further improve the performance of perovskite-based solar cells, more efforts on the development of HTM in terms of electronic properties and oxidation potentials are highly needed. The most popular HTM in perovskite solar cells is spiro-OMeTAD. O-methoxy substituents in spiro-OMeTAD kindly adjusted the electronic properties of this material and boosted the PCE of mesoporous-structured solar cells based on $MAPbI_3$ as light absorber to 16.7 % [130]. Hole conducting polymers (HCPs) are also good choices. Compared with spiro-OMeTAD and other small molecules [131] that are often expensive, HCPs are more cost-effective. Heo et al. [71] employed PTAA as HTM in solar cells using $MAPbI_3$ as light absorber, achieving efficiency of 12.8 %. By exploring a series of PTAA derivatives containing fluorine and indenofluorene with

different HOMO levels, Ryu et al. [73] further increased the performance to 16.2 % using $MAPbI_3$ as the light absorber. In additions to these efforts made on organic HTM, inorganic HTMs are also explored for perovskite solar cells to improve the stability of devices. Among them, Qin et al. [75] deposited a layer of CuSCN by doctor blading method on top of $MAPbI_3$ as HTM in combination with TiO_2 mesoporous layer as ETM achieving a high efficiency of over 12 %. Another popular inorganic p-type semiconductor is copper iodide (CuI). Christians et al. [132] constructed CuI solar cells via an automated drop-casting technique for the deposition of CuI on top of $MAPbI_3/TiO_2$ layer and got an efficiency of 6 %. The low performance was reported to be caused by the high recombination in CuI devices.

The biggest challenges of commercialization of perovskite solar cells are still the usage of lead as well the long-term stability. Improved stability of lead perovskite solar cells has been reported by Mei et al. [92] who fabricated a perovskite solar cell that used a simple mesoscopic $TiO_2/ZrO_2/C$ triple layer as a scaffold to host the perovskite absorber. Although lead-free perovskites have been recently reported, the high instability of tin-based perovskites in ambient atmospheres requires the whole assembly procedures of tin-based solar cells inside an inert atmosphere, such as N_2- or Ar-filled glovebox, which largely inhibits industrialization of this type of solar cells. Other lead-free perovskites with better stability in air and strong light harvesting ability will have more potential in applications in solar cells. In addition, non-perovskite materials with small band gaps, such as Sb_2S_3 or CuZnSnS that have been widely used as light absorbers in thin film solar cells, may also show possibilities in the substitution of lead perovskites. Considering the very short research history of these new types of perovskite solar cells yet the tremendous improvement in conversion efficiency from merely 3.8 % to over 20 % in 5 years, we should have very good hope that the new generation low-cost and high-efficiency solar cells could pave a new way to sustainable utilization of renewable solar energy.

Acknowledgments This work was supported by the Australian Research Council (ARC) through Discovery Project programs. We also acknowledge the technical support from the Queensland node of the Australian National Fabrication Facility.

Conflict of interest The authors declare that they have no conflict of interest.

References

1. Mitzi DB (2001) Templating and structural engineering in organic–inorganic perovskites. J Chem Soc Dalton Trans 1:1–12
2. Li C, Lu X, Ding W et al (2008) Formability of ABX_3 (X=F, Cl, Br, I) halide perovskites. Acta Crystallogr Sect B Struct Sci 64:702–707
3. Kawamura Y, Mashiyama H, Hasebe K (2002) Structural study on cubic-tetragonal transition of $CH_3NH_3PbI_3$. J Phys Soc Jpn 71:1694–1697
4. Yamada K, Kawaguchi H, Matsui T et al (1990) Structural phase-transition and electrical-conductivity of the perovskite $CH_3NH_3SN_{1-x}PB_xBR_3$ and $CSSNBR_3$. Bull Chem Soc Jpn 63:2521–2525
5. Koka A, Zhou Z, Sodano HA (2014) Vertically aligned $BaTiO_3$ nanowire arrays for energy harvesting. Energy Environ Sci 7:288–296
6. Yang SY, Martin LW, Byrnes SJ et al (2009) Photovoltaic effects in $BiFeO_3$. Appl Phys Lett 95:062909
7. Haeni JH, Irvin P, Chang W et al (2004) Room-temperature ferroelectricity in strained $SrTiO_3$. Nature 430:758–761
8. Grinberg I, West DV, Torres M et al (2013) Perovskite oxides for visible-light-absorbing ferroelectric and photovoltaic materials. Nature 503:509–512
9. Bowen CR, Kim HA, Weaver PM et al (2014) Piezoelectric and ferroelectric materials and structures for energy harvesting applications. Energy Environ Sci 7:25–44
10. Bretschneider SA, Weickert J, Dorman JA et al (2014) Research update: physical and electrical characteristics of lead halide perovskites for solar cell applications. APL Mater 2:040701
11. Unger EL, Hoke ET, Bailie CD et al (2014) Hysteresis and transient behavior in current-voltage measurements of hybrid-perovskite absorber solar cells. Energ Environ Sci 7:3690–3698
12. Snaith HJ, Abate A, Ball JM et al (2014) Anomalous hysteresis in perovskite solar cells. J Phys Chem Lett 5:1511–1515
13. McGehee MD (2014) Perovskite solar cells: continuing to soar. Nat Mater 13:845–846
14. Frost JM, Butler KT, Walsh A (2014) Molecular ferroelectric contributions to anomalous hysteresis in hybrid perovskite solar cells. APL Mater 2:081506
15. Kim HS, Park NG (2014) Parameters affecting *I–V* hysteresis of $CH_3NH_3PbI_3$ perovskite solar cells: effects of perovskite crystal size and mesoporous TiO_2 layer. J Phys Chem Lett 5:2927–2934
16. Kutes Y, Ye L, Zhou Y et al (2014) Direct observation of ferroelectric domains in solution-processed $CH_3NH_3PbI_3$ perovskite thin films. J Phys Chem Lett 5:3335–3339
17. Kojima A, Teshima K, Shirai Y et al (2009) Organometal halide perovskites as visible-light sensitizers for photovoltaic cells. J Am Chem Soc 131:6050–6051
18. Oregan B, Grätzel M (1991) A low-cost, high-efficiency solar-cell based on dye-sensitized colloidal TiO_2 films. Nature 353:737–740
19. Wu X, Chen Z, Lu GQ et al (2011) Nanosized anatase TiO_2 single crystals with tunable exposed (001) facets for enhanced energy conversion efficiency of dye-sensitized solar cells. Adv Funct Mater 21:4167–4172
20. Bai Y, Yu H, Li Z et al (2012) In situ growth of a ZnO nanowire network within a TiO_2 nanoparticle film for enhanced dye-sensitized solar cell performance. Adv Mater 24:5850–5856
21. Wang Q, Butburee T, Wu X et al (2013) Enhanced performance of dye-sensitized solar cells by doping Au nanoparticles into photoanodes: a size effect study. J Mater Chem A 1:13524–13531
22. Campbell WM, Jolley KW, Wagner P et al (2007) Highly efficient porphyrin sensitizers for dye-sensitized solar cells. J Phys Chem C 111:11760–11762
23. Yella A, Lee HW, Tsao HN et al (2011) Porphyrin-sensitized solar cells with cobalt(II/III)–based redox electrolyte exceed 12 percent efficiency. Science 334:629–634
24. Mathew S, Yella A, Gao P et al (2014) Dye-sensitized solar cells with 13 % efficiency achieved through the molecular engineering of porphyrin sensitizers. Nat Chem 6:242–247

25. Im JH, Lee CR, Lee JW et al (2011) 6.5 % efficient perovskite quantum-dot-sensitized solar cell. Nanoscale 3:4088–4093
26. Wu X, Lu GQ, Wang L (2011) Shell-in-shell TiO_2 hollow spheres synthesized by one-pot hydrothermal method for dye-sensitized solar cell application. Energ Environ Sci 4:3565–3572
27. Kim HS, Lee CR, Im JH et al (2012) Lead iodide perovskite sensitized all-solid-state submicron thin film mesoscopic solar cell with efficiency exceeding 9 %. Sci Rep 2:591
28. Lee MM, Teuscher J, Miyasaka T et al (2012) Efficient hybrid solar cells based on meso-superstructured organometal halide perovskites. Science 338:643–647
29. Zhang WH, Cai B (2014) Organolead halide perovskites: a family of promising semiconductor materials for solar cells. Chin Sci Bull 59:2092–2101
30. Sum TC, Mathews N (2014) Advancements in perovskite solar cells: photophysics behind the photovoltaics. Energ Environ Sci 7:2518–2534
31. Gao P, Gratzel M, Nazeeruddin MK (2014) Organohalide lead perovskites for photovoltaic applications. Energ Environ Sci 7:2448–2463
32. Park NG (2013) Organometal perovskite light absorbers toward a 20 % efficiency low-cost solid-state mesoscopic solar cell. J Phys Chem Lett 4:2423–2429
33. Cardona M (1965) Optical properties and band structure of $SrTiO_3$ and $BaTiO_3$. Phys Rev 140:A651–A655
34. Salehi H, Shahtahmasebi N, Hosseini SM (2003) Band structure of tetragonal $BaTiO_3$. Eur Phys J B 32:177–180
35. Noh JH, Im SH, Heo JH et al (2013) Chemical management for colorful, efficient, and stable inorganic-organic hybrid nanostructured solar cells. Nano Lett 13:1764–1769
36. Era M, Morimoto S, Tsutsui T et al (1994) Organic–inorganic heterostructure electroluminescent device using a layered perovskite semiconductor $(C_6H_5C_2H_4NH_3)_2PbI_4$. Appl Phys Lett 65:676–678
37. Kitazawa N, Watanabe Y, Nakamura Y (2002) Optical properties of $CH_3NH_3PbX_3$ (X=halogen) and their mixed-halide crystals. J Mater Sci 37:3585–3587
38. Ishihara T (1994) Optical properties of PbI-based perovskite structures. J Lumines 60–61:269–274
39. Wehrenfennig C, Liu M, Snaith HJ et al (2014) Homogeneous emission line broadening in the organo lead halide perovskite $CH_3NH_3PbI_{3-x}Cl_x$. J Phys Chem Lett 5:1300–1306
40. Deschler F, Price M, Pathak S et al (2014) High photoluminescence efficiency and optically pumped lasing in solution-processed mixed halide perovskite semiconductors. J Phys Chem Lett 5:1421–1426
41. Xing G, Mathews N, Lim SS et al (2014) Low-temperature solution-processed wavelength-tunable perovskites for lasing. Nat Mater 13:476–480
42. Zhang M, Yu H, Lyu M et al (2014) Composition-dependent photoluminescence intensity and prolonged recombination lifetime of perovskite $CH_3NH_3PbBr_{3-x}Cl_x$ films. Chem Commun 50:11727–11730
43. Stranks SD, Eperon GE, Grancini G et al (2013) Electron-hole diffusion lengths exceeding 1 micrometer in an organometal trihalide perovskite absorber. Science 342:341–344
44. Xing G, Mathews N, Sun S et al (2013) Long-range balanced electron- and hole-transport lengths in organic–inorganic $CH_3NH_3PbI_3$. Science 342:344–347
45. Noel NK, Abate A, Stranks SD et al (2014) Enhanced photoluminescence and solar cell performance via Lewis base passivation of organic–inorganic lead halide perovskites. ACS Nano 8:9815–9821
46. Oga H, Saeki A, Ogomi Y et al (2014) Improved understanding of the electronic and energetic landscapes of perovskite solar cells: high local charge carrier mobility, reduced recombination, and extremely shallow traps. J Am Chem Soc 136:13818–13825
47. Etgar L, Gao P, Xue Z et al (2012) Mesoscopic $CH_3NH_3PbI_3/TiO_2$ heterojunction solar cells. J Am Chem Soc 134:17396–17399
48. Zhou H, Shi Y, Dong Q et al (2014) Hole-conductor-free, metal-electrode-free $TiO_2/CH_3NH_3PbI_3$ heterojunction solar cells based on a low-temperature carbon electrode. J Phys Chem Lett 5:3241–3246
49. Edri E, Kirmayer S, Mukhopadhyay S et al (2014) Elucidating the charge carrier separation and working mechanism of $CH_3NH_3PbI_{3-x}Cl_x$ perovskite solar cells. Nat Commun 5:3461
50. Wang Q, Yun JH, Zhang M et al (2014) Insight into the liquid state of organo-lead halide perovskites and their new roles in dye-sensitized solar cells. J Mater Chem A 2:10355–10358
51. Liu M, Johnston MB, Snaith HJ (2013) Efficient planar heterojunction perovskite solar cells by vapour deposition. Nature 501:395–398
52. Kumar MH, Yantara N, Dharani S et al (2013) Flexible, low-temperature, solution processed ZnO-based perovskite solid state solar cells. Chem Commun 49:11089–11091
53. Kim J, Kim G, Kim TK et al (2014) Efficient planar-heterojunction perovskite solar cells achieved via interfacial modification of a sol-gel ZnO electron collection layer. J Mater Chem A 2:17291–17296
54. Loh L, Briscoe J, Dunn S (2014) Enhanced performance with bismuth ferrite perovskite in ZnO nanorod solid state solar cells. Nanoscale 6:7072–7078
55. Robel I, Subramanian V, Kuno M et al (2006) Quantum dot solar cells. Harvesting light energy with CdSe nanocrystals molecularly linked to mesoscopic TiO_2 films. J Am Chem Soc 128:2385–2393
56. Ramos FJ, Lopez-Santos MC, Guillen E et al (2014) Perovskite solar cells based on nanocolumnar plasmadeposited ZnO thin films. Chem Phys Chem 15:1148–1153
57. Son DY, Im JH, Kim HS et al (2014) 11 % efficient perovskite solar cell based on ZnO nanorods: an effective charge collection system. J Phys Chem C 118:16567–16573
58. Edri E, Kirmayer S, Henning A et al (2014) Why lead methylammonium tri-iodide perovskite-based solar cells require a mesoporous electron transporting scaffold (but not necessarily a hole conductor). Nano Lett 14:1000–1004
59. Du J, Qi J, Wang D et al (2012) Facile synthesis of Au@TiO_2 core-shell hollow spheres for dye-sensitized solar cells with remarkably improved efficiency. Energy Environ Sci 5:6914–6918
60. Dong Z, Ren H, Hessel CM et al (2014) Quintuple-shelled SnO_2 hollow microspheres with superior light scattering for high-performance dye-sensitized solar cells. Adv Mater 26:905–909
61. Dong Z, Lai X, Halpert JE et al (2012) Accurate control of multishelled ZnO hollow microspheres for dye-sensitized solar cells with high efficiency. Adv Mater 24:1046–1049
62. Zhang Q, Dandeneau CS, Zhou X et al (2009) ZnO nanostructures for dye-sensitized solar cells. Adv Mater 21:4087–4108
63. Zhang Q, Chou TP, Russo B et al (2008) Aggregation of ZnO nanocrystallites for high conversion efficiency in dye-sensitized solar cells. Angew Chem Int Edit 47:2402–2406
64. Chou TP, Zhang Q, Fryxell GE et al (2007) Hierarchically structured ZnO film for dye-sensitized solar cells with enhanced energy conversion efficiency. Adv Mater 19:2588–2592
65. De Wolf S, Holovsky J, Moon SJ et al (2014) Organometallic halide perovskites: sharp optical absorption edge and its relation to photovoltaic performance. J Phys Chem Lett 5:1035–1039
66. Ono LK, Wang S, Kato Y et al (2014) Fabrication of semi-transparent perovskite films with centimeter-scale superior uniformity by the hybrid deposition method. Energy Environ Sci 7:3989–3993
67. Conings B, Baeten L, Jacobs T et al (2014) An easy-to-fabricate low-temperature TiO_2 electron collection layer for high efficiency planar heterojunction perovskite solar cells. APL Mater 2:081505

68. Ke WJ, Fang G, Wang J et al (2014) Perovskite solar cell with an efficient TiO_2 compact film. ACS Appl Mater Inter 6:15959–15965
69. Wu YZ, Yang X, Chen H et al (2014) Highly compact TiO_2 layer for efficient hole-blocking in perovskite solar cells. Appl Phys Express 7:052301
70. Bach U (2000) Solid-state dye-sensitized mesoporous TiO_2 solar cells. Dissertation, University of Konstanz
71. Heo JH, Im SH, Noh JH et al (2013) Efficient inorganic-organic hybrid heterojunction solar cells containing perovskite compound and polymeric hole conductors. Nat Photonics 7:486–491
72. Liu XZ, Luo YH, Li H et al (2007) Room temperature fabrication of porous ZnO photoelectrodes for flexible dye-sensitized solar cells. Chem Commun 27:2847–2849
73. Ryu S, Noh JH, Jeon NJ et al (2014) Voltage output of efficient perovskite solar cells with high open-circuit voltage and fill factor. Energy Environ Sci 7:2614–2618
74. Zhu Z, Bai Y, Lee HKH et al (2014) Polyfluorene derivatives are high-performance organic hole-transporting materials for inorganic-organic hybrid perovskite solar cells. Adv Funct Mater 24:7357–7365
75. Qin P, Tanaka S, Ito S et al (2014) Inorganic hole conductor-based lead halide perovskite solar cells with 12.4 % conversion efficiency. Nat Commun 5:3834
76. Christians JA, Fung RCM, Kamat PV (2013) An inorganic hole conductor for organo-lead halide perovskite solar cells. Improved hole conductivity with copper iodide. J Am Chem Soc 136:758–764
77. Brabec CJ, Cravino A, Meissner D et al (2001) Origin of the open circuit voltage of plastic solar cells. Adv Funct Mater 11:374–380
78. Li G, Zhu R, Yang Y (2012) Polymer solar cells. Nat Photonics 6:153–161
79. Wirix MJM, Bomans PHH, Friedrich H et al (2014) Three-dimensional structure of P3HT assemblies in organic solvents revealed by cryo-TEM. Nano Lett 14:2033–2038
80. Snaith HJ, Moule AJ, Klein C et al (2007) Efficiency enhancements in solid-state hybrid solar cells via reduced charge recombination and increased light capture. Nano Lett 7:3372–3376
81. Snaith HJ, Grätzel M (2007) Electron and hole transport through mesoporous TiO_2 infiltrated with spiro-MeOTAD. Adv Mater 19:3643–3647
82. Snaith HJ, Grätzel M (2007) Light-enhanced charge mobility in a molecular hole transporter. Phys Rev Lett 98:177402
83. Yang L, Xu B, Bi D et al (2013) Initial light soaking treatment enables hole transport material to outperform spiro-OMeTAD in solid-state dye-sensitized solar cells. J Am Chem Soc 135:7378–7385
84. Dittrich T, Kieven D, Rusu M et al (2008) Current-voltage characteristics and transport mechanism of solar cells based on ZnO nanorods/In_2S_3/CuSCN. Appl Phys Lett 93:053113
85. Kieven D, Dittrich T, Belaidi A et al (2008) Effect of internal surface area on the performance of ZnO/In_2S_3/CuSCN solar cells with extremely thin absorber. Appl Phys Lett 92:153107
86. Page M, Niitsoo O, Itzhaik Y et al (2009) Copper sulfide as a light absorber in wet-chemical synthesized extremely thin absorber (ETA) solar cells. Energ Environ Sci 2:220–223
87. Itzhaik Y, Niitsoo O, Page M et al (2009) Sb_2S_3-sensitized nanoporous TiO_2 solar cells. J Phys Chem C 113:4254–4256
88. Liu D, Yang J, Kelly TL (2014) Compact layer free perovskite solar cells with 13.5 % efficiency. J Am Chem Soc 136:17116
89. Shi J, Luo Y, Wei H et al (2014) Modified two-step deposition method for high-efficiency TiO_2/$CH_3NH_3PbI_3$ heterojunction solar cells. ACS Appl Mater Inter 6:9711–9718
90. Laban WA, Etgar L (2013) Depleted hole conductor-free lead halide iodide heterojunction solar cells. Energy Environ Sci 6:3249–3253
91. Aharon S, Gamliel S, El Cohen BE et al (2014) Depletion region effect of highly efficient hole conductor free $CH_3NH_3PbI_3$ perovskite solar cells. Phys Chem Chem Phys 16:10512–10518
92. Mei A, Li X, Liu L et al (2014) A hole-conductor-free, fully printable mesoscopic perovskite solar cell with high stability. Science 345:295–298
93. Eperon GE, Burlakov VM, Docampo P et al (2014) Morphological control for high performance, solution-processed planar heterojunction perovskite solar cells. Adv Funct Mater 24:151–157
94. Dualeh A, Tétreault N, Moehl T et al (2014) Effect of annealing temperature on film morphology of organic–inorganic hybrid perovskite solid-state solar cells. Adv Funct Mater 24:3250–3258
95. Burschka J, Pellet N, Moon SJ et al (2013) Sequential deposition as a route to high-performance perovskite-sensitized solar cells. Nature 499:316–319
96. Liang K, Mitzi DB, Prikas MT (1998) Synthesis and characterization of organic–inorganic perovskite thin films prepared using a versatile two-step dipping technique. Chem Mater 10:403–411
97. Wu Y, Islam A, Yang X et al (2014) Retarding the crystallization of PbI_2 for highly reproducible planar-structured perovskite solar cells via sequential deposition. Energ Environ Sci 7:2934–2938
98. Bi D, El-Zohry AM, Hagfeldt A et al (2014) Improved morphology control using a modified two-step method for efficient perovskite solar cells. ACS Appl Mater Inter 6:18751–18757
99. Kim HB, Choi H, Jeong J et al (2014) Mixed solvents for the optimization of morphology in solution-processed, inverted-type perovskite/fullerene hybrid solar cells. Nanoscale 6:6679–6683
100. Xiao M, Huang F, Huang W et al (2014) A Fast deposition-crystallization procedure for highly efficient lead iodide perovskite thin-film solar cells. Angew Chem Int Ed 53:9898–9903
101. Jeon NJ, Noh JH, Kim YC et al (2014) Solvent engineering for high-performance inorganic-organic hybrid perovskite solar cells. Nat Mater 13:897–903
102. Salau AM (1980) Fundamental absorption edge in PbI_2:KI alloys. Sol Energy Mater 2:327–332
103. Era M, Hattori T, Taira T et al (1997) Self-organized growth of PbI-based layered perovskite quantum well by dual-source vapor deposition. Chem Mater 9:8–10
104. Mitzi DB, Prikas MT, Chondroudis K (1999) Thin film deposition of organic–inorganic hybrid materials using a single source thermal ablation technique. Chem Mater 11:542–544
105. Chen Q, Zhou H, Hong Z et al (2013) Planar heterojunction perovskite solar cells via vapor-assisted solution process. J Am Chem Soc 136:622–625
106. Xiao Z, Bi C, Shao Y et al (2014) Efficient, high yield perovskite photovoltaic devices grown by interdiffusion of solution-processed precursor stacking layers. Energy Environ Sci 7:2619–2623
107. Huang F, Dkhissi Y, Huang W et al (2014) Gas-assisted preparation of lead iodide perovskite films consisting of a monolayer of single crystalline grains for high efficiency planar solar cells. Nano Energy 10:10–18
108. Ball JM, Lee MM, Hey A et al (2013) Low-temperature processed meso-superstructured to thin-film perovskite solar cells. Energy Environ Sci 6:1739–1743
109. Wojciechowski K, Saliba M, Leijtens T et al (2014) −150 °C processed meso-superstructured perovskite solar cells with enhanced efficiency. Energy Environ Sci 7:1142–1147
110. Docampo P, Ball JM, Darwich M et al (2013) Efficient organometal trihalide perovskite planar-heterojunction solar cells on flexible polymer substrates. Nat Commun 4:2761
111. Yu H, Wang F, Xie F et al (2014) The role of chlorine in the formation process of "$CH_3NH_3PbI_{3-x}Cl_x$" perovskite. Adv Funct Mater 24:7102–7108

112. Zuo C, Ding L (2014) An 80.11 % FF record achieved for perovskite solar cells by using the NH_4Cl additive. Nanoscale 6:9935–9938
113. Williams ST, Zuo F, Chueh CC et al (2014) Role of chloride in the morphological evolution of organo-lead halide perovskite thin films. ACS Nano 8:10640–10654
114. Mosconi E, Amat A, Nazeeruddin MK et al (2013) First-principles modeling of mixed halide organometal perovskites for photovoltaic applications. J Phys Chem C 117:13902–13913
115. Aharon S, Cohen BE, Etgar L (2014) Hybrid lead halide iodide and lead halide bromide in efficient hole conductor free perovskite solar cell. J Phys Chem C 118:17160–17165
116. Feng J, Xiao B (2014) Crystal structures, optical properties, and effective mass tensors of $CH_3NH_3PbX_3$ (X=I and Br) phases predicted from HSE06. J Phys Chem Lett 5:1278–1282
117. Chen J, Xu L, Li W et al (2005) α-Fe_2O_3 nanotubes in gas sensor and lithium-ion battery applications. Adv Mater 17:582–586
118. Edri E, Kirmayer S, Kulbak M et al (2014) Chloride inclusion and hole transport material doping to improve methyl ammonium lead bromide perovskite-based high open-circuit voltage solar cells. J Phys Chem Lett 5:429–433
119. Eperon GE, Stranks SD, Menelaou C et al (2014) Formamidinium lead trihalide: a broadly tunable perovskite for efficient planar heterojunction solar cells. Energy Environ Sci 7:982–988
120. Pang S, Hu H, Zhang J et al (2014) $NH_2CH{=}NH_2PbI_3$: an alternative organolead iodide perovskite sensitizer for mesoscopic solar cells. Chem Mater 26:1485–1491
121. Hanusch FC, Fabian C, Wiesenmayer E et al (2014) Efficient planar heterojunction perovskite solar cells based on formamidinium lead bromide. J Phys Chem Lett 5:2791–2795
122. Lv S, Pang S, Zhou Y et al (2014) One-step, solution-processed formamidinium lead trihalide ($FAPbI_{3-x}Cl_x$) for mesoscopic perovskite-polymer solar cells. Phys Chem Chem Phys 16:19206–19211
123. Smith IC, Hoke ET, Solis-Ibarra D et al (2014) A layered hybrid perovskite solar-cell absorber with enhanced moisture stability. Angew Chem Int Ed 126:11414–11417
124. Gratzel M (2014) The light and shade of perovskite solar cells. Nat Mater 13:838–842
125. Noel NK, Nakita K, Stranks SD et al (2014) Lead-free organic–inorganic tin halide perovskites for photovoltaic applications. Energy Environ Sci 7:3061–3068
126. Hao F, Stoumpos CC, Cao DH et al (2014) Lead-free solid-state organic–inorganic halide perovskite solar cells. Nat Photonics 8:489–494
127. Chung I, Song JH, Im J et al (2012) $CsSnI_3$: semiconductor or metal? High electrical conductivity and strong near-infrared photoluminescence from a single material. High hole mobility and phase-transitions. J Am Chem Soc 134:8579–8587
128. Chung I, Lee B, He J et al (2012) All-solid-state dye-sensitized solar cells with high efficiency. Nature 485:486–489
129. Kumar MH, Mulmudi H, Dharani S et al (2014) Lead-free halide perovskite solar cells with high photocurrents realized through vacancy modulation. Adv Mater 26:7122–7127
130. Jeon NJ, Lee HG, Kim YC et al (2014) O-methoxy substituents in spiro-OMeTAD for efficient inorganic-organic hybrid perovskite solar cells. J Am Chem Soc 136:7837–7840
131. Qin P, Paek S, Dar MI et al (2014) Perovskite solar cells with 12.8 % efficiency by using conjugated quinolizino acridine based hole transporting material. J Am Chem Soc 136:8516–8519
132. Christians JA, Fung RCM, Kamat PV (2013) An inorganic hole conductor for organo-lead halide perovskite solar cells improved hole conductivity with copper iodide. J Am Chem Soc 136:758–764